Novel Hierarchical Porous Carbon for Fabrications of Ru/NHPC Catalysts with the High Hydrogen Evolution Reaction Performance

OPEN ACCESS

Wantao ZHANG,[a] Xifei ZHOU,[a,*] Beibei HAN,[b,c] Xiaofei GUO,[d] Yi ZHOU,[d] Baigang AN,[a] Kun WANG,[a,*]
Guiying XU,[a,*] Lixiang LI,[a] Maorong CHAI,[b,e] Dongying JU,[a,f] and Weimin ZHOU[a,*,§] 🔴

[a] *Key Laboratory of Energy Materials and Electrochemistry Research Liaoning Province, University of Science and Technology Liaoning, No. 189 Qianshan Middle Road, Lishan District, Anshan City, Liaoning Province, Anshan 114051, China*

[b] *Advanced Science Research Laboratory, Saitama Institute of Technology, 1690 Fusaiji, Fukaya 369-0293, Japan*

[c] *Key Laboratory of Advanced Fuel Cells and Electrolyzers Technology of Zhejiang Province, Ningbo Institute of Materials Technology and Engineering, Chinese Academy of Sciences, Ningbo, No. 1219 Zhongguan West Road, Zhejiang 315201, China*

[d] *Liaoning Huarong Furui New Energy Technology Co., Ltd., Angbao, Dadaowan, Qianshan District, Anshan 114020, Liaoning, China*

[e] *State Power Investment Corporation Hydrogen Energy Co., Ltd., Building 2, Yard 15, Xinya Street, Daxing District, Beijing 102600, China*

[f] *Hainan University, 58 Renmin Avenue, Haikou 570228, China*

* *Corresponding authors: aszhou15242870697@163.com (W. Z.), 672253324@qq.com (X. Z.), xuguiying751107@163.com (G. X.), ustl15542731203@163.com (K. W.)*

ABSTRACT

To enhance the performance of Ru in hydrogen evolution reaction (HER), the design and fabrication of catalytic supports become one of the critical research topics. Carbon supports possessing the excellent conductivity and remarkable cost advantage have become one of the primary choices in fabrications of composite catalysts. In our present studies, the NHPC (N-doped hierarchical porous carbon) supports are fabricated by the carbonizations of soluble starch, ammonium citrate and sodium bicarbonate, and the Ru/NHPC catalysts are successfully prepared by the reactions of $RuCl_3 \cdot 3H_2O$ with $NaBH_4$ and NHPC in the ultrasonic treatment. As a result, it is found that Ru goodly dispersed on the surfaces of NHPC in nano sizes, and the Ru/NHPC catalysts manifest the fabulous HER performance. For instance, the overpotential of 11.2 %Ru/NHPC (the loading of $RuCl_3 \cdot 3H_2O$ is 0.05 g) is 33 mV at a current density of 10 mA cm^{-2}, which is remarkably lower than 48 mV of glassy carbon electrode (20 %Pt/C) in alkaline medium (1 M (mol L^{-1}) KOH). The Tafel slope of 11.2 %Ru/NHPC is 36 mV dec^{-1} at 10 mA cm^{-2} in the same conditions. Although the 11.2 %Ru/NHPC is in the acidic medium (0.5 M H_2SO_4), it also displays the routine HER performance. In short, this present study provides a useful approach to facilitate the application of Ru as a hydrogen evolution catalyst.

Keywords : Hydrogen Evolution Reaction (HER), N-doped Hierarchical Porous Carbon (NHPC), Ru Catalyst, Carbon Supports

1. Introduction

To date, over using fossil energy has caused the serious environmental deterioration on a world-wide scale.[1–4] Developing green energy is becoming an extremely urgent task in the world. Hydrogen energy has attracted more attention than ever before due to its resource advantage and high energy density. In comparison with the pyrolysis of fossil raw material and biomass, water electrolysis is an effective way to obtain green hydrogen.[5–7] Nevertheless, in the general electrolytic process, the slow kinetic curves of HER and large over-potential of catalysts lead to a slow rate of water electrolysis and an appearance of unnecessary energy consumption. Thus, it is necessary to develop the catalysts with the high electrocatalytic performance so as to address the aforementioned issues.

In particular, noble metals, non-noble metals and nonmetals are used to increase the efficiency of water electrolysis.[8–13] Among them, catalysts using the non-noble metals are difficult to be applied in the HER process because their hydrogen adsorption ability is not available.[14,15] Because of the fact that Pt has the good hydrogen binding energy, it manifests the excellent HER performance, causing that it is widely used as a standard material for HER. However, the reserves of Pt and reactive differences in acidic and alkaline environments restrict its wide application in the fabrication of

catalysts for HER.[16,17] Besides, it is well known that Ru is a relatively inexpensive metal, and Ru also possesses the excellent hydrogen binding energy, similar to Pt. Additionally, the ideal anti-corrosion characteristic property of Ru further expands its applicable perspective.[18]

Although the Ru catalyst possesses the strong catalytic performance, various demerits such as high dissolution rate, and agglomeration problems have to be addressed in practical applications.[19,20] Generally, three courses are developed and utilized to improve the catalytic performance. (**i**) The particle sizes of noble metals are decreased as far as possible, in order to increase the density of accessible active centers. (**ii**) Improving the intrinsic activity of catalyst is realized by optimizing the structures of catalysts.[21–25] (**iii**) Designing excellent catalyst support makes catalysts develop their catalyst activity enough. The excellent support materials are able to diminish the usages of catalysts, leading to a decrease in cost. In addition, the activity and stability of catalysts can be improved, through improving dispersions of catalysts on the surfaces of catalyst supports.[26–28] Among many catalyst supports such as carbon black, carbon nanotubes, and MOF materials, the carbon materials with hierarchical porous structures have become the research focus due to their high specific surface area and rich pore structures.[29–31] Additionally, N doped carbon materials with hierarchical porous structures can increase the active sites not only, but the interactions between catalyst and supports can also be strengthened.[32]
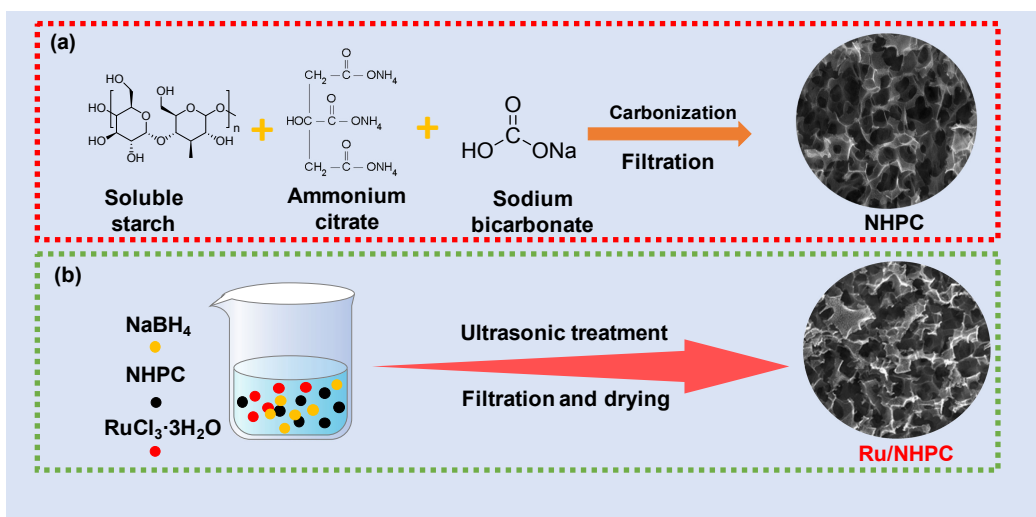
Figure 1. Schematic illustration of fabrication procedures of NHPC and Ru/NHPC materials.

Based on the above mentioned research status, we adopted the starch as a carbon source and used a strategy of "leavening" to fabricate the N doped hierarchical porous carbon materials.[33,34] As a result, the Ru/NHPC catalysts are fabricated by the way that the Ru catalysts are homogeneously dispersed on the surface of NHPC materials by using the ultrasonic assisted deposition method. It is observed that the fabricated catalysts possess large specific surface area and complex porous structures, which are beneficial to the exposure of active sites, acceleration of mobility of electrolytes and release of hydrogen.

After carrying out the evaluations of HER performance, it is found that the fabricated Ru/NHPC catalysts possess the excellent catalytic performance in alkaline conditions. For instance, the overpotential is 33 mV, and the Tafel slope is 36 mV dec^{-1} at 10 mA cm^{-2} in 1 M KOH solution. Besides, it is found that the overpotential is 76 mV, and the Tafel slope is 48 mV dec^{-1} at 10 mA cm^{-2} in 0.5 M H$_2$SO$_4$ electrolyte. Although the HER performance of 11.2 %Ru/NHPC (the loading of RuCl$_3$·3H$_2$O is 0.05 g) in the acidic condition is not ideal, it is close to the level of 20 %Pt/C. These results suggest that fabricated Ru/NHPC catalysts owning relatively wide usage conditions are the expected materials that can be applied in HER fields as a catalyst.

2. Experimental

2.1 Characterizations

The measurements of X-ray diffraction (XRD) were performed by the X'pert powder instrument from PANalytical. The X-ray photoelectron spectroscopy (XPS) measurements were carried out on a K-Alpha instrument from Thermo Fisher Scientific, USA. Nitrogen adsorption and desorption isotherms were measured by a Quadrasorbautosorb-iQ surface analyzer which was purchased from Quantachrome Instruments, USA. Specific surface areas were determined in detail, according to the Brunauer-Emmett-Teller (BET) method. The pore size distribution was assessed by a density functional theory (DFT) model for slit pores. Morphology was evaluated by transmission electron microscopy (TEM) using JEOL-JEM-2010F instruments, Japan. Thermogravimetric (TG) analysis (TG209F3, NETZSCH Group, Germany) was conducted from 30 °C to 700 °C at a heating rate of 10 °C per minute in air.

2.2 Fabrications of NHPC (N-doped hierarchically porous carbon)

The soluble starch (2.0 g), ammonium citrate (6.0 g) and sodium bicarbonate (6.0 g) were added to a beaker, and mixed homogeneously. The obtained solid mixture was placed in a tube furnace with nitrogen purging, and the temperature of the tube furnace was increased to 800 °C with a heating rate of 10 °C/min, and then maintained at 800 °C for 1 h. When cooling down to room temperature, the obtained carbon materials were added to a beaker with the deionized water (500 ml), and this mixture was stirred for 2 h. Finally, the homogeneous mixture was filtered, and the obtained solid was washed by deionized water until the pH value of the washed solution became neutral. The final obtained solids were dried in a drying oven at 80 °C for 12 h, and the NHPC was collected (Fig. 1a).

2.3 Fabrications of Ru/NHPC catalysts

RuCl$_3$·3H$_2$O (0.05 g) and NHPC (0.10 g) were added to a beaker. After adding the deionized water (500 mL) to the same beaker, the sonicated mixture was dealt with by ultrasonic for 10 min. The NaBH$_4$ (25 mL) of 2 mg/ml was slowly dropped in the aforementioned mixture. Contiguously, this mixture was dealt with by ultrasonic for 30 min at room temperature. Finally, this mixture was filtered, and then washed by deionized water and anhydrous alcohol 3 times. The obtained solids were placed in a dying oven and dried at 80 °C for 12 h (Fig. 1b).

Similarly, the dosages of RuCl$_3$·3H$_2$O and NaBH$_4$ (2 mg/ml) were adjusted to (0.02 g, 10 mL) and (0.10 g, 50 mL), respectively. After carrying out the same synthesis process, the Ru/NHPC composts were also fabricated. Finally, all of the fabricated Ru/NHPC catalysts were respectively named as 10.2 %Ru/NHPC, 11.2 %Ru/NHPC and 24.7 %Ru/NHPC, according to the loading of Ru on the surface of NHPC.

2.4 Electrochemical measurements

The electrochemical measurements were conducted by a three-electrode system. The glassy carbon electrode, platinum electrodes and Hg/HgO or Ag/AgCl are the working electrode, counter electrode and reference electrode, respectively. The 1 M KOH and 0.5 M H$_2$SO$_4$ are the electrolytes, which were treated with by N$_2$ bubbling for 30 min. The homogenous catalyst ink was constructed by the catalysts (5 mg), isopropanol (700 µL), deionized water (200 µL) and Nafion solution with 0.5 wt% (100 µL), and this ink was treated by the ultrasonic for 30 min, in order to disperse the catalysts in solution homogeneously. Subsequently, the homogeneous catalyst ink was placed on the surface of the glassy carbon electrode which was clearly treated beforehand. The glassy carbon

electrodes were dried at room temperature. All of the measurement data were calibrated by references on the reversible hydrogen electrode (RHE) with an 80 % *IR* correction. In addition, the Ru/NHPC catalysts were loaded on the glassy carbon electrode at $0.0025 \, g/cm^2$.

The detailed electrochemical measurements were described as the following. Firstly, the electrodes were carried out the activation treatment by CV (scanning rate: $100 \, mV \, s^{-1}$) at the hydrogen evolution potential ranges of $-1.6 \, V$–$0.8 \, V$ in the alkaline condition and $-0.7 \, V$–$0 \, V$ in the acidic condition. Subsequently, the linear sweep voltammetry (LSV) measurements were performed with a scanning rate of $5 \, mV \, s^{-1}$ at a potential range of $-1.6 \, V$–$0.8 \, V$ (in the alkaline condition) and $-0.7 \, V$–$0 \, V$ (in the acidic condition). Electrochemical impedance spectroscopy (EIS) measurements were performed at a frequency range of $10^5 \, Hz$–$10^{-1} \, Hz$ with an amplitude of $5 \, mV$. The electrochemical stability of the catalyst was investigated by carrying out the LSV measurements 1000 cycles at potential ranges of $-1.6 \, V$–$0.8 \, V$ in the alkaline condition and $-0.7 \, V$–$0 \, V$ in the acidic condition. Meanwhile, the chronoamperometry was used to evaluate the electrochemical stability at $10 \, mA \, cm^{-2}$.

3. Results and Discussion

The structures of Ru/NHPC catalysts were investigated by XRD measurements in detail (Fig. 2). It is obvious that two broad peaks of 22° and 43° can be attributed to characteristic peaks of carbon supports, revealing that the carbons exist as the amorphous state. Compared to a standard of ICDD 01-089-3942 of Ru, it is considerable that the peaks of 38.38°, 42.19°, 44.02°, 58.35°, 69.41°, 78.41°, 82.21°, 84.69° and 85.95° correspond to the lattice planes of (002), (101), (102), (110), (103), (200), (112) and (201) of Ru, respectively. Furthermore, with increasing the dosages of $RuCl_3 \cdot 3H_2O$, the intensities of characteristic peaks of Ru become stronger, indicating that a more prominent of Ru was immobilized on the surface of carbon supports.[35]

The structures of Ru/NHPC catalysts were further analyzed by the Raman measurements (Fig. 3). Similarly, the D peak attributing to the defects on the graphite edge and G peak from the sp^2 structures on carbon shifts were observed at $1355 \, cm^{-1}$ and $1600 \, cm^{-1}$, respectively.[36,37] Additionally, the intensity ratios (I_D/I_G) of D and G peaks can reflect the disorder degree and surface defects. The I_D/I_G values of NHPC, 10.2 %Ru/NHPC, 11.2 %Ru/NHPC and 24.7 %Ru/NHPC are 1.18, 1.19, 1.18 and 1.16, respectively, as shown in Table S1, suggesting that dispersing Ru on the surfaces of NHPC had little to no effect on the NHPC structural integrity.
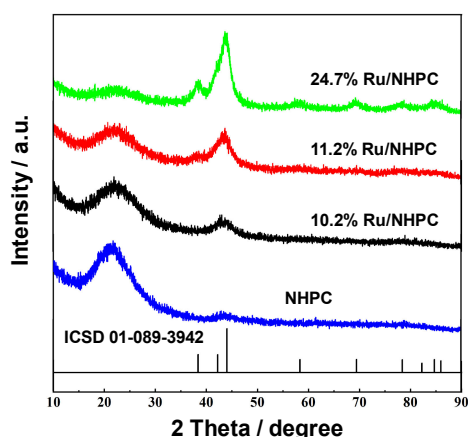

Figure 2. XRD patterns of NHPC and Ru/NHPC with different Ru contents.
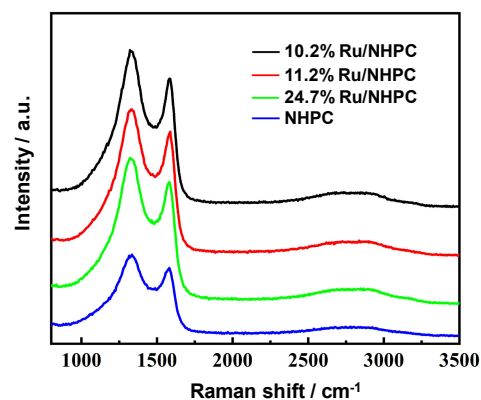

Figure 3. Raman spectra of NHPC and Ru/NHPC with different Ru contents.

To inquire into the morphologies and structures of NHPC and Ru/NHPC catalysts, the SEM and TEM measurements were performed thoroughly (Fig. 4). Figure 4b clearly demonstrated that Ru/NHPC catalysts possess distinct hierarchical porous structures. The SEM-EDS images indicate that N and Ru elements are homogeneously dispersed on the surface of the carbon supports of NHPC (Figs. 4e–4g). The HRTEM images of 11.2 %Ru/NHPC show that the sizes of Ru are around 2.5 nm (Fig. 4j), and the lattice fringe spacing is 0.214 nm which corresponds to the (002) plane of the hexagonal close-packed (hcp) Ru.[38] In addition, compared to the 11.2 %Ru/NHPC and 24.7 %Ru/NHPC, the lattice fringe images of 10.2 %Ru/NHPC are not distinct, suggesting that the degree of crystallinity increased with the dosages of $RuCl_3$ in reaction cases (Figs. 4l–4m). This tendency is consistent with the results of XRD measurements.

After carrying out the evaluations of BET methods, it is found that all samples show a type IV isotherm with type H1 hysteresis loops, indicating the existences of mesoporous structures (Fig. S1a).[39] As shown in Table S2, the specific surface areas of NHPC, 10.2 %Ru/NHPC, 11.2 %Ru/NHPC and 24.7 %Ru/NHPC are $1392.08 \, m^2 \, g^{-1}$, $1082.92 \, m^2 \, g^{-1}$, $1023.23 \, m^2 \, g^{-1}$ and $859.84 \, m^2 \, g^{-1}$, respectively, revealing that the specific surface areas decrease with a rise in the catalyst loading amount. The pore size distribution curves exhibit that Ru/NHPC catalysts possess a lot of micropores (1.17 nm) and mesopores (2.53 nm) (Fig. S1b). As mentioned above, the relatively high specific surface areas of NHPC supports are beneficial to disperse the Ru catalyst, and complex pore structures are conducive to transfer the electrolytes.

The chemical states of Ru/NHPC were investigated by the XPS measurements. As per the Fig. 5a, it is found that peaks of C, N, O, and Ru of 11.2 %Ru/NHPC were 248.8 eV, 400.5 eV, 532.0 eV and 462.5 eV, respectively, suggesting that 11.2 %Ru/NHPC was constructed by the C, N, O, and Ru elements. The fitting method is used to further investigate the detailed chemical states of elements. As shown in Fig. 5b, two peaks of 280.4 eV and 280.8 eV can be ascribed to the Ru^0 and Ru^{n+} belonging to the Ru-N bonds.[26] This result suggests that the doped N element has a coordination effect on the Ru, which increases the reaction activity of Ru. It is observed that three peaks of 398.5 eV, 400.5 eV and 401.9 eV are the characteristic peaks of pyridine-N, pyrrole-N, and graphitic N, respectively (Fig. 5c). The nitrogen functionalities on the surface are expected to enrich the electron density of the metallic Ru atom.[40–42] The fitting peaks of Ru 3p were illustrated as shown in Fig. 5d. The $3p_{3/2}$ and $3p_{1/2}$ of Ru^0 of 11.2 %Ru/NHPC were observed at 462.5 eV and 484.6 eV, respectively. Meanwhile, the peaks of 465.8 eV and 487.2 eV respectively corresponding to the $3p_{3/2}$ and $3p_{1/2}$ of Ru^{n+} were also observed in the 11.2 %Ru/NHPC. The characteristic peaks of Ru $3p_{3/2}$ and $3p_{1/2}$ were also observed in
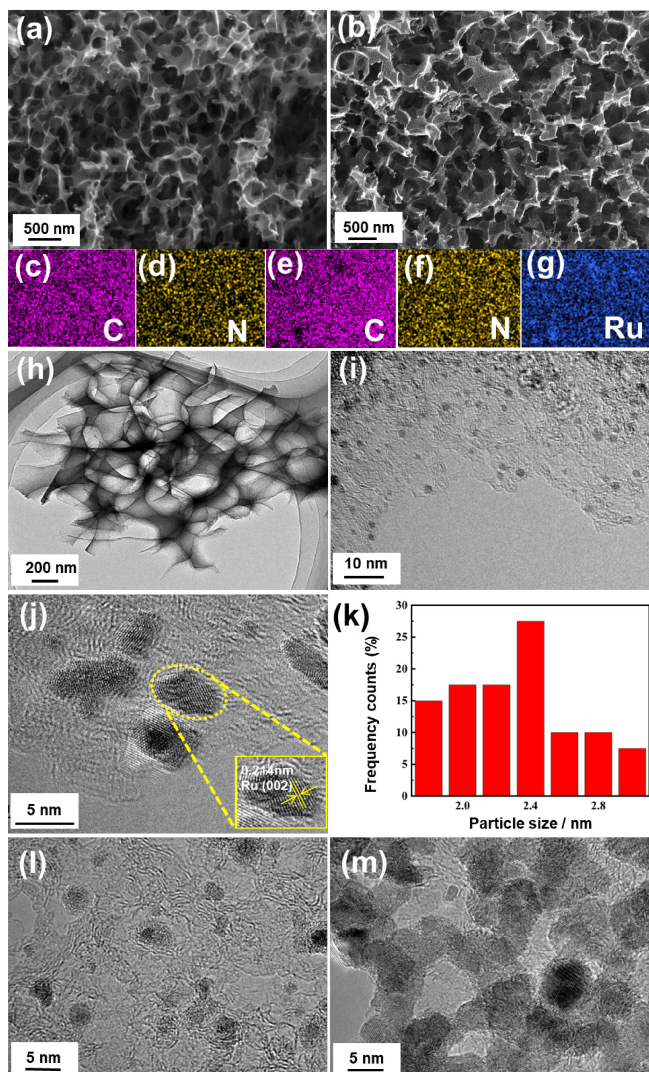
Figure 4. SEM images of NHPC (a) and 11.2 %Ru/NHPC (b). (c) and (d) are the EDS images of NHPC. (e), (f) and (g) are EDS images of 11.2 %Ru/NHPC. TEM images of NHPC (h). (i)–(j) are the HRTEM images of 11.2 %Ru/NHPC. (k) is the corresponding metal particle size distribution histograms of (i). (l)–(m) are the HRTEM images of 10.2 %Ru/NHPC and 24.7 %Ru/NHPC.

10.2 %Ru/NHPC and 24.7 %Ru/NHPC materials (Figs. 5e–5f). Additionally, after carrying out calculations, the peak area ratio of Ru^0 (462.5 eV, 484.6 eV) with Ru^{n+} (465.8 eV, 487.2 eV) in the 11.2 %Ru/NHPC is around 70 %, which is higher than that in 10.2 %Ru/NHPC (54.4 %) and 24.7 %Ru/NHPC (60 %), respectively. To further investigate the Ru^0 amount in the Ru/NHPC, the TG measurements were conducted. As shown in Fig. S2, the mass losses before 100 °C are naturally attributed to the water loss, and remarkable mass losses occurring at a temperature range of (100 °C–500 °C) are ascribed to the burning of carbons in the Ru/NHPC. After calculations, the contents of Ru in the Ru/NHPC are 10.2 %, 11.2 %, and 24.7 %, respectively. The TG results indicate that the contents of Ru in Ru/NHPC show an increase trend, with increasing dosages of $RuCl_3$. In addition, associated with the ratios of Ru^0/Ru^{n+} by XPS results, the Ru^0 contents in 10.2 %Ru/NHPC, 11.2 %Ru/NHPC and 24.7 %Ru/NHPC were calculated as 3.6 %, 4.7 %, and 9.3 %, respectively.

Although the contents of Ru^0 in 24.7 %Ru/NHPC are higher than that of 11.2 %Ru/NHPC, the lower specific surface area of 24.7 %Ru/NHPC (859.84 m^2/g) causes that the agglomeration phenomenon among the Ru^0 in 24.7 %Ru/NHPC is stronger than

that in 11.2 %Ru/NHPC and 10.2 %Ru/NHPC, respectively. A relatively serious agglomeration phenomenon of 24.7 %Ru/NHPC could be observed in Fig. 4m. The aforementioned analyses and results indicate that the content of the independent Ru^0 in Ru/NHPC catalysts is an important factor in enhancing the HER performance of Ru/NHPC catalysts. On the present stage, the percentage of Ru^0/Ru^{n+} on the surface could be only controlled by adjusting the weight ratios of $RuCl_3·3H_2O$ with $NaBH_4$ and NHPC in reactions.

The HER performances of Ru/NHPC catalysts in 1 M KOH were firstly performed by the three-electrode system (Fig. 6). The overpotential of 10.2 %Ru/NHPC, 11.2 %Ru/NHPC and 24.7 %Ru/NHPC were 49 mV, 33 mV and 46 mV at a current density of 10 mA cm^{-2}, respectively, indicating that 11.2 %Ru/NHPC possesses the more excellent HER performance than the others (Fig. 6a). Furthermore, the overpotential of 11.2 %Ru/NHPC is 33 mV at a current density of 10 mA cm^{-2}, which is remarkably lower than the 48 mV of glassy carbon electrode (20 %Pt/C) (Fig. 6b).

The catalytic activities of 20 %Pt/C and Ru/NHPC catalysts were further evaluated by the Tafel slopes. As shown in Fig. 6c, the 20 %Pt/C, 10.2 %Ru/NHPC, 11.2 %Ru/NHPC and 24.7 %Ru/NHPC manifested the Tafel slopes at 46 mV dec^{-1}, 55 mV dec^{-1}, 36 mV dec^{-1} and 80 mV dec^{-1}, respectively, which also suggests that 11.2 %Ru/NHPC owns the best catalytic activity, compared with the 20 %Pt/C and other Ru/NHPC catalysts. The overpotentials and Tafel slopes of 20 %Pt/C, 10.2 %Ru/NHPC, 11.2 %Ru/NHPC and 24.7 %Ru/NHPC were comprehensively illustrated in the Fig. 6d. It is observed that the 11.2 %Ru/NHPC possesses the more excellent HER performance than the other Ru/NHPC catalysts in our studies and reported catalysts containing Ru (Table S3).

The stability of 11.2 %Ru/NHPC in 1 M KOH was evaluated by CV and chronoamperometry measurements. It is observed that two polarization curves before and after 1000 cycles overlapped approximately, indicating that 11.2 %Ru/NHPC owns remarkable electrochemical stability (Fig. 7). The chronoamperometry measurement also exhibits that 11.2 %Ru/NHPC shows the excellent stability for 12 h under a potential of 33 mV (inset in Fig. 7).

The capacitances of the double layer at the solid-liquid interface (C_{dl}) were derived by the cyclic voltammetry (CV) curves of 20 %Pt/C and 11.2 %Ru/NHPC at scanning rates of 20, 40, 60, 80, 100 and 120 mV s^{-1} in KOH (1 M), respectively (Figs. 8a–8b). The relationships between the scanning rates and the half of the capacitive current are illustrated in the Fig. 8c. After calculating by CV measurements, it is aware of that the capacitance of the double layer at the solid-liquid interface (C_{dl}) of 11.2 %Ru/NHPC is 44.6 mF cm^{-2}, which is higher than the C_{dl} 24.8 mF cm^{-2} of 20 %Pt/C.

EIS measurements were used to evaluate the kinetic characteristics of 20 %Pt/C and Ru/NHPC catalysts in 1 M KOH. Figure 8d exhibited that 11.2 %Ru/NHPC possessed the smaller diameters of semicircle loop at a high frequency region than 20 %Pt/C and other Ru/NHPC materials, suggesting that 11.2 %Ru/NHPC showed a more excellent conductivity than the others. In addition, the R_{ct} values of 20 %Pt/C, 10.2 %Ru/NHPC, 11.2 %Ru/NHPC and 24.7 %Ru/NHPC were simulated and determined with values of 6.8 Ω, 13.9 Ω, 6.5 Ω and 8.5 Ω, respectively, revealing that the 11.2 %Ru/NHPC owns more marvelous charge transfer properties (Table S4). Associated with the analyses of XPS and BET, it is considered that more notable dispersion of Ru^0 and complex porous structures lead to the fabulous charge transfer properties of 11.2 %Ru/NHPC.

Likewise, the HER performances of Ru/NHPC and 20 %Pt/C catalysts in an electrolyte solution of 0.5 M H_2SO_4 were thoroughly investigated. As shown in Figs. S3a–S3b, the overpotentials of 10.2 %Ru/NHPC, 11.2 %Ru/NHPC, 24.7 %Ru/NHPC and
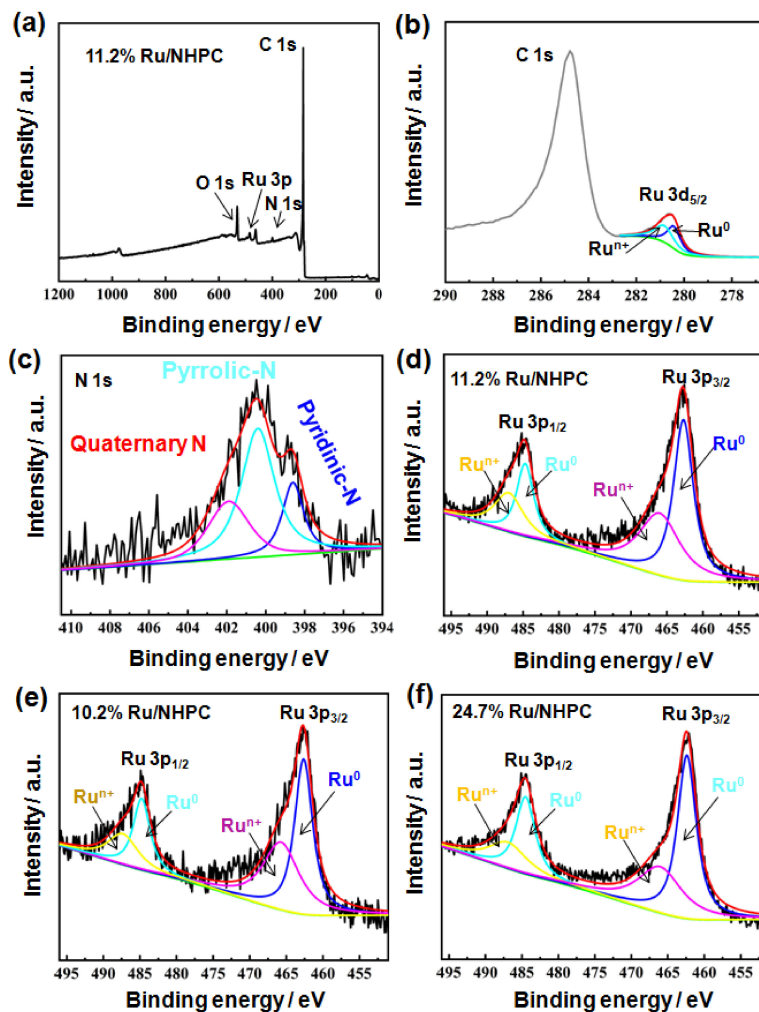
Figure 5. XPS results. XPS survey spectrum of 11.2 %Ru/NHPC (a). High-resolution XPS spectra of C 1s + Ru 3d$_{5/2}$ (b), N 1s (c) and Ru 3p of 11.2 %Ru/NHPC (d). High-resolution XPS spectra of Ru 3p of 10.2 %Ru/NHPC (e) and 24.7 %Ru/NHPC (f).
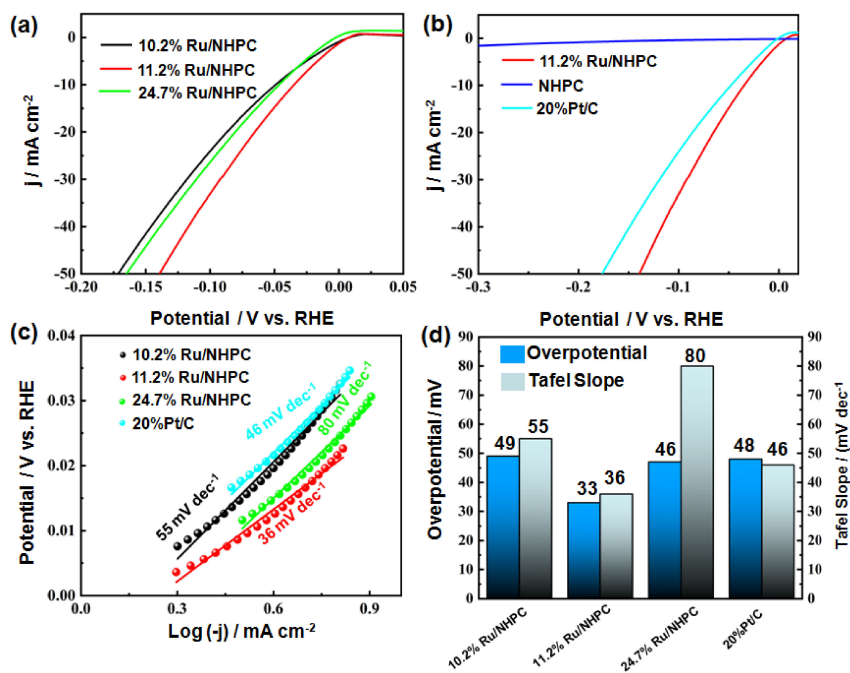

Figure 6. Electrochemical measurements of HER performances in alkaline medium. HER polarization curves of Ru/NHPC with different Ru contents in 1 M KOH (a). HER performances of commercial 20 %Pt/C, NHPC and 11.2 %Ru/NHPC in 1 M KOH (b). (c) are the Tafel plots obtained from the polarization curves in (a) and (b). Corresponding statistical chart of overpotentials and Tafel slopes (d).
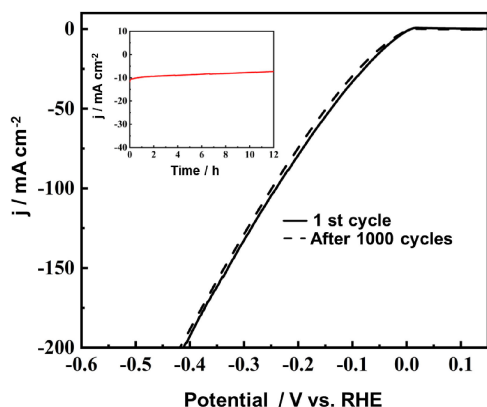
Figure 7. Stability test of 11.2 %Ru/NHPC by 1000 potential cycles in 1 M KOH (The inset is stability test at a constant potential of 0.033 V for 12 h.).

20 %Pt/C were 125 mV, 76 mV, 84 mV and 30 mV, respectively. Meanwhile, the 10.2 %Ru/NHPC, 11.2 %Ru/NHPC, 24.7 %Ru/NHPC and 20 %Pt/C exhibited the Tafel slopes at 72 mV dec^{-1}, 48 mV dec^{-1}, 87 mV dec^{-1} and 31 mV dec^{-1} at a current density of 10 mA cm^{-2}, respectively (Fig. S3c). The overpotential and Tafel slope results were also comprehensively illustrated in (Fig. S3d). The aforementioned results indicate that 11.2 %Ru/NHPC has better HER properties than that of the other Ru/NHPC materials in 0.5 M H$_2$SO$_4$, however, the HER performance of 11.2 %Ru/NHPC is inferior to the 20 %Pt/C.

The stability of 11.2 %Ru/NHPC in 0.5 M H$_2$SO$_4$ was also evaluated by CV and chronoamperometry measurements. Compared with the initial LSV measurement, it is found that there is a slight left-shift (17 mV) of overpotential of 11.2 %Ru/NHPC after carrying out CV measurements 1000 cycles, revealing that 11.2 %Ru/NHPC owns electrochemical stability to a great extent.

The chronoamperometry measurement exhibits that 11.2 %Ru/NHPC possesses excellent stability for 12 h under a potential of 76 mV (Fig. S4).

The CV measurements about 11.2 %Ru/NHPC and 20 %Pt/C were conducted under a potential range (0.1–0.23 V) with changing the scan rates from 20 to 120 mV s^{-1} in 0.5 M H$_2$SO$_4$. The relationships between the scan rates and current densities were obtained, in accordance with CV measurements (Figs. S5a–S5b). After calculations, the C$_{dl}$ values of 11.2 %Ru/NHPC and 20 %Pt/C are 38.4 mF cm^{-2} and 29.8 mF cm^{-2}, respectively, suggesting that the electrochemical activity of 11.2 %Ru/NHPC approaches to the 20 %Pt/C in the acidic condition (Fig. S5c).

The conductivities of 11.2 %Ru/NHPC and 20 %Pt/C were finally conducted by the electrochemical impedance spectroscopy (EIS) measurements (Fig. S5d). After simulations, the R$_{ct}$ of 10.2 %Ru/NHPC, 11.2 %Ru/NHPC, 24.7 %Ru/NHPC and 20 %Pt/C were determined with values of 10.1 Ω, 16.9 Ω, 13.2 Ω and 15.1 Ω, respectively, indicating that 11.2 %Ru/NHPC possesses the similar conductivity to the 20 %Pt/C in 0.5 M H$_2$SO$_4$ (Table S5). The fact that 11.2 %Ru/NHPC shows a more excellent HER performance in the alkaline medium than that in the acidic medium indicates that N-doping is an effective way to enhance the HER performance of Ru on the NHPC surfaces because the H$^+$ probably decreases the contribution of N on the NHPC surfaces.

4. Conclusions

Ru/NHPC catalysts with high HER performance were successfully fabricated by dispersing the Ru on the surfaces of NHPC carbon supports which are fabricated by carbonizations of soluble starch, ammonium citrate and sodium bicarbonate. It is found that fabricated 11.2 %Ru/NHPC possesses the more impressive HER performance in the 1 M KOH electrolyte than that in 0.5 M H$_2$SO$_4$ electrolyte. For instance, the overpotential of 11.2 %Ru/NHPC is 33 mV at a current density of 10 mA cm^{-2}, which is remarkably
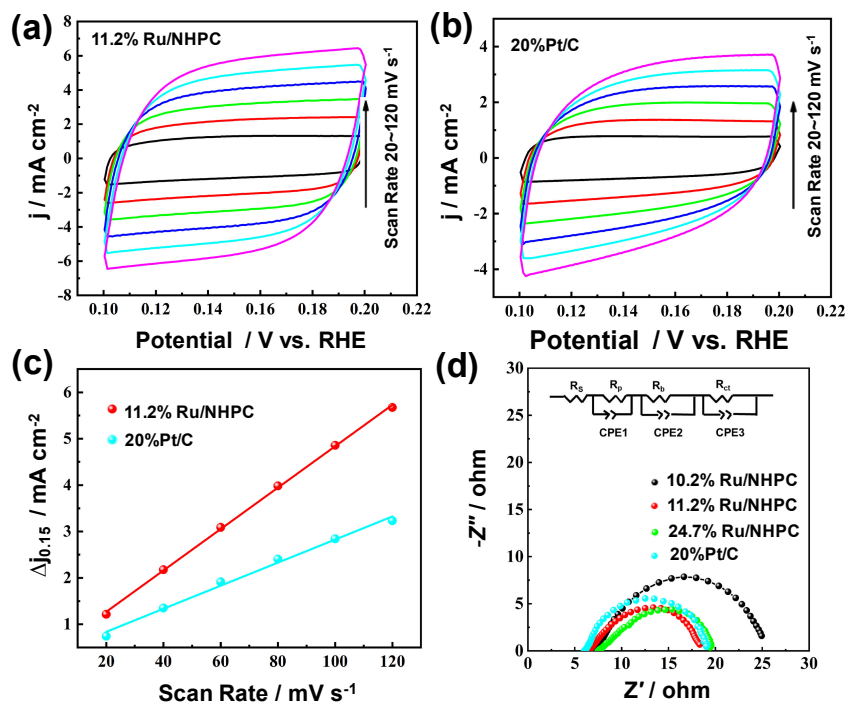

Figure 8. C$_{dl}$ measurements from cycles voltammetry in 1 M KOH of 11.2 %Ru/NHPC (a), 20 %Pt/C (b). Current versus scan rate for 11.2 %Ru/NHPC and 20 %Pt/C (c). Nyquist plots of 20 %Pt/C and Ru/NHPC with different Ru contents (d). In this model, Rs represents the electric resistance of the solution, wires and the contact resistance between the glassy carbon electrode and the catalysts, and the Rs connects in series with three additional branches: one relates to the surface porosity (R$_p$), another one relates to the bulk resistance (R$_b$), the third one relates to the charge-transfer process (R$_{ct}$). The CPE1, CPE2 and CPE3 belong to constant phase element of the electrode-electrolyte interface.

lower than the 48 mV of glassy carbon electrode (20 %Pt/C). The Tafel slope of 11.2 %Ru/NHPC is 36 mV dec^{-1} at 10 mA cm^{-2} in 1 M KOH solution, which is lower than the 48 mV dec^{-1} of 20 %Pt/C under the same conditions. It is also observed that 11.2 %Ru/NHPC exhibits more excellent HER performance in 1 M KOH electrolyte than that in 0.5 M H$_2$SO$_4$. Although the HER performance of 11.2 %Ru/NHPC in the acidic condition is not ideal, but it is close to the level of 20 %Pt/C. These results suggest that fabricated Ru/NHPC materials own relatively wide usage conditions, suggesting that fabricated Ru/NHPC catalysts possess the extremely desirable prospect in the applications of fabrications of fuel cells.

Acknowledgments

CRediT Authorship Contribution Statement

Wantao Zhang: Data curation (Equal), Investigation (Lead), Writing – original draft (Lead)

Xifei Zhou: Data curation (Equal), Investigation (Equal), Writing – original draft (Supporting)

Beibei Han: Formal analysis (Equal), Investigation (Equal)

Xiaofei Guo: Project administration (Lead), Resources (Lead)

Yi Zhou: Project administration (Equal), Resources (Equal)

Baigang An: Project administration (Equal), Supervision (Equal)

Kun Wang: Investigation (Lead), Methodology (Equal)

Guiying Xu: Formal analysis (Lead), Investigation (Equal), Methodology (Equal)

Lixiang Li: Methodology (Equal), Project administration (Equal)

Maorong Chai: Project administration (Equal), Supervision (Lead)

Dongying Ju: Project administration (Equal), Resources (Equal), Supervision (Supporting)

Weimin Zhou: Conceptualization (Lead), Writing – review & editing (Lead)

Data Availability Statement

The data that support the findings of this study are openly available under the terms of the designated Creative Commons License in J-STAGE Data listed in D1 of References.

Conflict of Interest

The authors declare no conflict of interest in the manuscript.

References

D1. W. Zhang, X. Zhou, B. Han, X. Guo, Y. Zhou, B. An, K. Wang, G. Xu, L. Li, M. Chai, D. Ju, and W. Zhou, *J-STAGE Data*, https://doi.org/10.50892/data.electrochemistry.24137892, (2023).

1. X. L. Yan, P. Duan, F. W. Zhang, H. Li, H. X. Zhang, M. Zhao, X. M. Zhang, B. S. Xu, S. J. Pennycook, and J. J. Guo, *Carbon*, **143**, 378 (2019).

2. H. Zhang, H. Su, M. A. Soldatov, Y. L. Li, X. Zhao, M. H. Liu, W. L. Zhou, X. X. Zhang, X. Sun, Y. Z. Xu, P. Yao, S. Q. Wei, and Q. H. Liu, *Small*, **17**, 2105231 (2021).

3. G. Q. Zhao, Y. Z. Jiang, S. X. Dou, W. P. Sun, and H. G. Pan, *Sci. Bull.*, **66**, 85 (2021).

4. M. G. Hosseini, P. Zardari, and I. Ariankhah, *J. Iran. Chem. Soc.*, **16**, 1749 (2019).

5. Z. D. Ren, Y. Q. Han, N. Cong, L. Z. Jin, L. J. Tan, H. R. Chen, C. H. Zhai, X. R. Zhou, H. Fang, and Y. C. Zhu, *J. Electroanal. Chem.*, **848**, 113320 (2019).

6. Y. S. Wu, X. J. Liu, D. D. Han, X. Y. Song, L. Shi, Y. Song, S. W. Niu, Y. F. Xie, J. Y. Cai, S. Y. Wu, J. Kang, J. B. Zhou, Z. Y. Chen, X. S. Zheng, X. H. Xiao, and G. M. Wang, *Nat. Commun.*, **9**, 1425 (2018).

7. J. F. Callejas, C. G. Read, C. W. Roske, N. S. Lewis, and R. E. Schaak, *Chem. Mater.*, **28**, 6017 (2016).

8. X. L. Sui, L. Zhang, J. J. Li, K. Doyle-Davis, R. Y. Li, Z. B. Wang, and X. L. Sun, *Adv. Energy Mater.*, **12**, 2102556 (2022).

9. M. D. Hossain, Z. J. Liu, M. H. Zhuang, X. X. Yan, G. L. Xu, C. A. Gadre, A. Tyagi, I. H. Abidi, C. J. Sun, H. L. Wong, A. Guda, Y. F. Hao, X. Q. Pan, K. Amine, and Z. T. Luo, *Adv. Energy Mater.*, **9**, 1803689 (2019).

10. Y. A. Polozhentseva, V. A. Bykov, A. M. Timonov, and M. P. Karushev, *Nanotechnol. Russ.*, **15**, 730 (2020).

11. L. Yu, W. Song, B. McElhenny, F. Z. Ding, D. Luo, Y. Yu, S. Chen, and Z. F. Ren, *J. Mater. Chem. A*, **7**, 19728 (2019).

12. J. Theerthagiri, S. J. Lee, A. P. Murthy, J. Madhavan, and M. Y. Choi, *Curr. Opin. Solid State Mater. Sci.*, **24**, 100805 (2020).

13. J. Yu, Y. N. Guo, S. X. She, S. S. Miao, M. Ni, W. Zhou, M. Liu, and Z. P. Shao, *Adv. Mater.*, **30**, 1800047 (2018).

14. H. B. Yu, L. L. Qi, Y. Hu, Y. Qu, P. X. Yan, T. T. Isimjan, and X. L. Yang, *J. Colloid Interface Sci.*, **600**, 811 (2021).

15. X. C. Li, H. M. You, C. Wang, D. M. Liu, R. Yu, S. Y. Guo, Y. Wang, and Y. K. Du, *J. Colloid Interface Sci.*, **591**, 203 (2021).

16. X. L. Tian, X. F. Lu, B. Y. Xia, and X. W. Lou, *Joule*, **4**, 45 (2020).

17. S. Zhang, C. Wang, X. Y. Zhang, H. Y. Xia, B. L. Huang, S. J. Guo, J. Li, and E. Wang, *ACS Appl. Mater. Interfaces*, **13**, 32997 (2021).

18. J. Yu, Q. J. He, G. M. Yang, W. Zhou, Z. P. Shao, and M. Ni, *ACS Catal.*, **9**, 9973 (2019).

19. S. Zhang, J. Li, and E. Wang, *ChemElectroChem*, **7**, 4526 (2020).

20. Y. L. Li, J. F. He, W. R. Cheng, H. Su, C. L. Li, H. Zhang, M. H. Liu, W. L. Zhou, X. Chen, and Q. H. Liu, *Sci. China Mater.*, **64**, 2467 (2021).

21. H. Li, C. Chen, D. F. Yan, Y. Y. Wang, R. Chen, Y. Q. Zou, and S. Y. Wang, *J. Mater. Chem. A*, **7**, 23432 (2019).

22. J. Zhang, Q. Y. Zhang, and X. L. Feng, *Adv. Mater.*, **31**, 1808167 (2019).

23. Y. Shi, Y. Zhou, D. R. Yang, W. X. Xu, C. Wang, F. B. Wang, J. J. Xu, X. H. Xia, and H. Y. Chen, *J. Am. Chem. Soc.*, **139**, 15479 (2017).

24. X. M. Li, X. G. Hao, A. Abudula, and G. Q. Guan, *J. Mater. Chem. A*, **4**, 11973 (2016).

25. Z. H. Pu, I. S. Amiinu, Z. K. Kou, W. Q. Li, and S. C. Mu, *Angew. Chem., Int. Ed.*, **56**, 11559 (2017).

26. Y. J. Li, H. J. Liu, B. Li, Z. Z. Yang, Z. G. Guo, J. B. He, J. H. Xie, and T. C. Lau, *J. Mater. Chem. A*, **9**, 12196 (2021).

27. J. S. Li, M. J. Huang, L. X. Kong, X. N. Chen, Y. W. Zhou, J. L. Li, and M. Y. Wang, *Inorg. Chem.*, **59**, 930 (2020).

28. B. Z. Lu, L. Guo, F. Wu, Y. Peng, J. E. Lu, T. J. Smart, N. Wang, Y. Z. Finfrock, D. Morris, P. Zhang, N. Li, P. Gao, Y. Ping, and S. W. Chen, *Nat. Commun.*, **10**, 631 (2019).

29. Y. Peng, B. Z. Lu, L. Chen, N. Wang, J. E. Lu, Y. Ping, and S. W. Chen, *J. Mater. Chem. A*, **5**, 18261 (2017).

30. J. Guan, Z. P. Zhang, J. Ji, M. L. Dou, and F. Wang, *ACS Appl. Mater. Interfaces*, **9**, 30662 (2017).

31. D. J. Zhou, P. S. Li, W. W. Xu, S. Jawaid, J. Mohammed-Ibrahim, W. Liu, Y. Kuang, and X. M. Sun, *ChemNanoMat*, **6**, 336 (2020).

32. N. Mahmood, Y. D. Yao, J. W. Zhang, L. Pan, X. W. Zhang, and J. J. Zou, *Adv. Sci.*, **5**, 1700464 (2018).

33. J. Deng, T. Y. Xiong, F. Xu, M. M. Li, C. L. Han, Y. T. Gong, H. Y. Wang, and Y. Wang, *Green Chem.*, **17**, 4053 (2015).

34. S. Dutta, A. Bhaumik, and K. C.-W. Wu, *Energy Environ. Sci.*, **7**, 3574 (2014).

35. H. L. Jia, J. Zhao, Z. Y. Wang, R. X. Chen, and M. Y. Guan, *Dalton Trans.*, **50**, 15585 (2021).

36. Y. L. Cao, S. J. Mao, M. M. Li, Y. Q. Chen, and Y. Wang, *ACS Catal.*, **7**, 8090 (2017).

37. J. N. Tiwari, A. M. Harzandi, M. Ha, S. Sultan, C. W. Myung, H. J. Park, D. Y. Kim, P. Thangavel, A. N. Singh, and P. Sharma, *Adv. Energy Mater.*, **9**, 1900931 (2019).

38. J. T. Zhu, L. J. Cai, Y. D. Tu, L. F. Zhang, and W. J. Zhang, *J. Mater. Chem. A*, **10**, 15370 (2022).

39. N. Mohammadi, M. Najafi, and N. B. Adeh, *Sens. Actuators, B*, **243**, 838 (2017).

40. J. Mahmood, F. Li, S. M. Jung, M. S. Okyay, I. A. Ahmad, S. J. Kim, N. Park, H. Y. Jeong, and J. B. Baek, *Nat. Nanotechnol.*, **12**, 441 (2017).

41. J. Wang, Z. Z. Wei, S. J. Mao, H. R. Li, and Y. Wang, *Energy Environ. Sci.*, **11**, 800 (2018).

42. Y. Zheng, Y. Jiao, Y. H. Zhu, L. H. Li, Y. Han, Y. Chen, M. Jaroniec, and S. Z. Qiao, *J. Am. Chem. Soc.*, **138**, 16174 (2016).